ASM-HEMT: Industry Standard GaN HEMT Model for Power and RF Applications (Invited Paper)

S. Ghosh*, S. A. Ahsan**, S. Khandelwal***, A. Pampori*, R. Dangi* and Y. S. Chauhan*

* Nanolab, Dept. of Electrical Engineering, Indian Institute of Technology Kanpur
Kanpur 208016, India, sudip@iitk.ac.in
** Electrical and Computer Engineering, NYU, NY 11201, USA
*** Department of Science and Engineering, Macquarie University, NSW 2109, Australia

ABSTRACT

An overview of a surface-potential (SP) based model for AlGaN/GaN HEMTs named "Advanced SPICE Model for High Electron Mobility Transistor" (ASM-HEMT) is presented in this paper. Recently, our model has been selected as industry standard model for GaN HEMTs by Si2-Compact Model Coalition (CMC) after more than five years of rigorous evaluation and testing by semiconductor companies. In our model, we preserve the 2DEG nature of the channel by self-consistently solving the Schrödinger's and Poisson's equations to obtain an analytical expression for the surface-potential after considering two energy sub-bands in the triangular quantum well at the hetero-interface. We proceed to calculate all other important quantities such as the intrinsic charges, drain current etc. in terms of the surface potential, valid for a wide range of bias conditions. We have incorporated real device effects such as Access Resistances, Drain Induced Barrier Lowering (DIBL), Mobility Degradation, Channel Length Modulation, Self-Heating, Gate Current, Noise, Field-Plates etc. We have a working trap model incorporated into the main model and it is validated against pulsed IV measurements, harmonic balance power sweeps and load pull for a commercial RF GaN HEMT. We have also validated the model for power devices with field plates and have been able to accurately capture the capacitances incorporated due to the field plates.

Keywords: AlGaN/GaN HEMTs, compact model, ASM-HEMT, SPICE model, Load-Pull.

1 Introduction

HEMTs based on GaN have become immensely ubiquitous in the past decade and offer a strong competition to mature technologies like silicon primarily due to the superior characteristics offered by the GaN material system over existing technologies [1]. A high bandgap allows the HEMT to perform under significantly higher voltages coupled with a high mobility two-dimensional electron gas (2DEG) allowing high power designs to be implemented in a considerably smaller area. The presence of the 2DEG, along with an undoped system which minimizes scattering, leads to a better frequency response and makes GaN HEMTs, candidates of choice for RF applications as well. Realizing these applications requires robust and computationally efficient model for these devices to be used in circuit simulation tools. The ASM-HEMT model presented in this paper is an effort in that direction. Among all the existing models for the GaN HEMT system [2–5], the ones based on surface potential [5] or intrinsic charges [4] are preferred owing to their physics-based formulation and scalability. The presence of these attributes allows these models to accurately simulate fairly complex systems both in the RF and power regimes. The primary goal of this paper is to provide a concise overview of the surface potential based ASM-HEMT model, which was recently selected as an industry standard by the CMC. This will involve demonstrating the robustness of the model across different sizes, bias conditions and operating temperatures.

2 Model Description

The ASM-HEMT model has its foundations based on the solution of the triangular potential well present at the heterostructure boundary of the AlGaN/GaN system. We obtain a self-consistent solution for the Fermi level of the system using Schrödinger's and Poisson's equations considering the first two sub-bands of the system. The solutions for the Fermi level are considered for different regions of operation of the device - based on the relative position of the Fermi level with the sub-bands. These regional solutions are then stitched together into a unified Fermi level expression given by [6]:

$$E_{f,unified} = V_{go} - \frac{2V_t ln\left(1 + e^{\frac{V_{go}}{2V_t}}\right)}{\frac{1}{H(V_{go,p})} + (C_g/qD)e^{-\frac{V_{go}}{2V_t}}} \quad (1)$$

where $V_{go} = V_{gs} - V_{OFF}$, V_{OFF} is the cut-off voltage, q is the electronic charge, C_g is the gate capacitance per unit area, D is the density of states and V_t is the thermal voltage. $H(V_{go,p})$ has been defined to capture the dependence of the Fermi level on applied bias for $V_{gs} > V_{OFF}$. $\psi = E_f + V_x$ then defines the surface potential of the device, where V_x is the channel potential.

Once we have the solution for the Fermi energy, 2DEG concentration for the channel is defined as $n = C_g(V_{go} -$

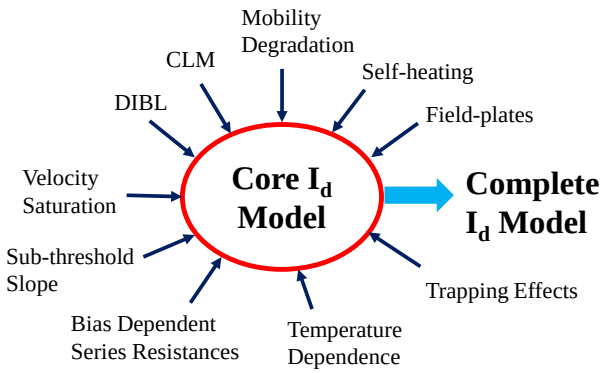

Figure 1: Schematic of ASM-HEMT complete drain-current model showing all the real device effects included along with the core drain current model.

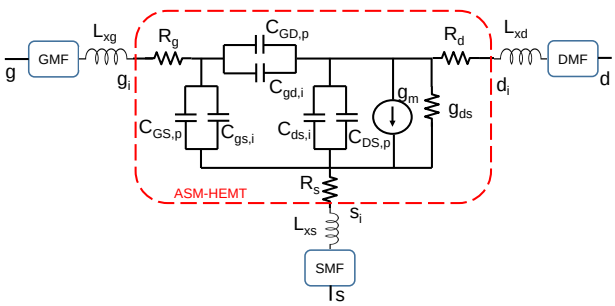

Figure 2: ASM-HEMT small-signal equivalent circuit model showing parasitic elements and the standard pad parasitics for simulations.

ψ) which is a function of both the applied voltage and the position in the channel. The charge stored in the entire channel is then derived by integrating this concentration over the dimensions of the device. Gate charge is then expressed as the channel charge with the opposite sign as [6]:

$$Q_g = -\int_0^L qWndx = -\int_0^L qWC_g(V_{go} - \psi)dx \quad (2)$$

Ward-Dutton partitioning scheme is then used to explicitly define the terminal charges in the device [7].

Since most of the contemporary GaN-HEMT devices have a fairly long channel length, the ASM-HEMT model uses a classical drift-diffusion model for transport. Drain current I_{ds} is calculated using the surface potential as [8]:

$$I_{ds} = \frac{\mu_{eff}C_g}{\sqrt{1+\theta_{sat}^2\psi_{ds}^2}}\frac{W}{L}\Big[(V_{go} - \psi_m + V_{th})(\psi_{ds}) (1+\lambda V_{ds,eff})\Big] \quad (3)$$

where $\psi_{ds} = \psi_d - \psi_s$ and $\psi_m = (\psi_d + \psi_s)/2$. Secondary effects like velocity saturation, vertical field dependence of mobility and channel length modulation are then incorporated using variables θ_{sat}, μ_{eff} and λ respectively. As depicted in Fig.1, two dimensional effects like DIBL

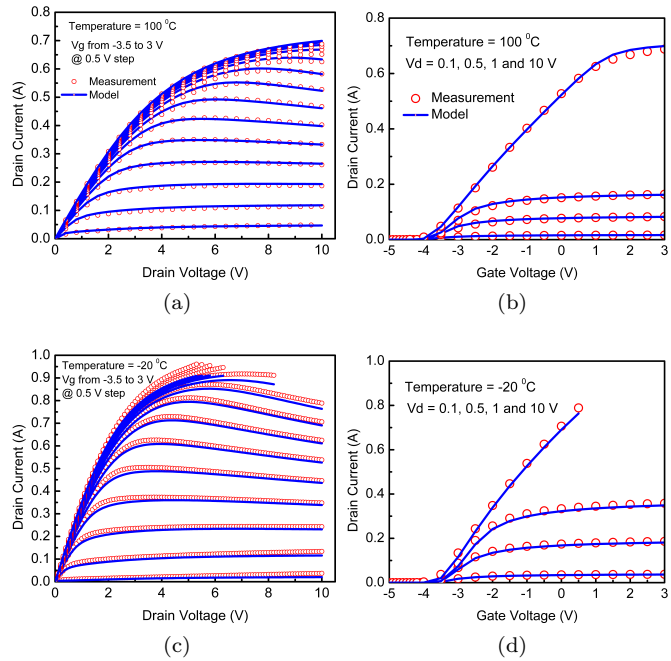

Figure 3: Modeling of output and transfer characteristics at two different temperatures: (a-b) 100 °C and (c-d) -20 °C. The non-linear $R_{d/s}$ and self-heating effects are accurately captured by the model which are visible at higher V_g.

have been incorporated in the model along with non-linear access region resistances, self-heating, temperature dependence etc. to accurately represent the characteristics of physically fabricated devices.

The access regions play a key role in both power and RF applications of the device by affecting breakdown-voltage (BV) and transit frequency (f_t). These regions exhibit a non-linear dependence on the current flowing through the device and effectively control the device characteristics at high gate voltages. ASM-HEMT represents these resistances using a current-dependent non-linear model as [9]:

$$R_{d/s} = \frac{R_{d0/s0}}{\left[1 - \left(\frac{I_d}{I_{acc,sat}}\right)^{\gamma}\right]^{\frac{1}{\gamma}}} \quad (4)$$

where $I_{acc,sat}$ is the maximum current supported in the access region and low current access resistance $R_{d0/s0} = L_{acc}/(Q_{acc} \cdot \mu_{acc})$. As is evident from (4), with I_d approaching $I_{acc,sat}$, $R_{d/s}$ increases rapidly and limits the total drain current flowing through the device.

ASM-HEMT incorporates physics-based models for across-the-spectrum noise - ranging from flicker noise [10] at low frequencies to thermal noise at high frequencies [11]. The former has been modeled taking into consideration both fluctuations in carrier density as well as mobility while the latter has been implemented using the approach by Klaassen and Prins. Gate-channel coupling is known to induce thermal noise in devices and has been modeled accordingly [12].

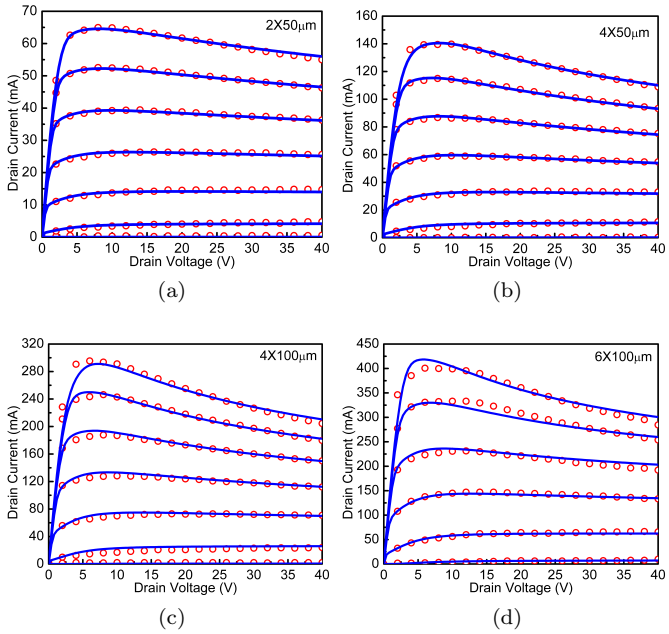

Figure 4: Scalable model extraction results for RF devices [17] with different widths and number of fingers, where thermal resistance parameter scaling is the key factor.

High power applications using GaN-HEMT devices can be significantly improved with the incorporation of field plates. While these appendages offer benefits in terms of breakdown voltage, the device capacitances are considerably increased as well. The presence of these capacitances has a key role in the application of a GaN HEMT as a switching device. Field plates have been modeled [13] in the ASM-HEMT model as series connected transistors with varying threshold voltages. Charge and current calculations for each of these transistors is modeled using the core ASM-HEMT formulation. The model also takes into account the cross-coupling charges induced due to fringing fields [14].

Capturing the temperature dependence of device characteristics is a key feature of all industry standard models and has been included in the core formulation (such as electron mobility, threshold voltage and saturation velocity) of the ASM-HEMT model. Further, the model also incorporates temperature dependence for $R_{d/s}$ [9, 16], gate current, field-plates and noise characteristics.

A key deciding factor for the RF performance of a system are its resistances and capacitances which decide its maximum operable frequency, gain and various other parameters. ASM-HEMT takes into account parasitic impedances both at the input (in the form of gate resistances and overlap capacitances) and the output of the device as can be seen in Fig. 2. RF applications also call for proper large signal modeling of device characteristics which requires a good trapping model.

The presence of traps significantly impacts the characteristics of a HEMT device, introducing effects like current collapse, and can be characterized using pulsed

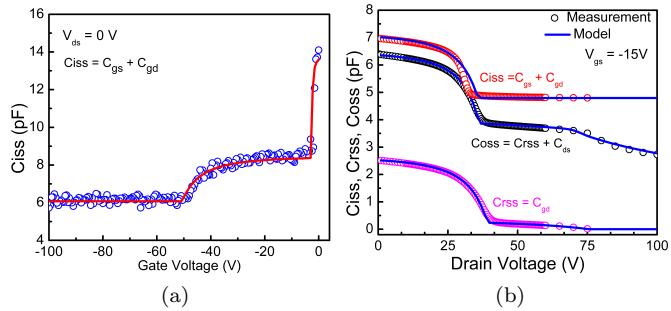

Figure 5: (a) Comparison of the modeled $Ciss - V_g$ with measured data at $V_d = 0V$ for the source and gate connected power GaN HEMT; (b) variation of input, reverse and output capacitances with V_d at sub-threshold condition ($V_g = -15V$).

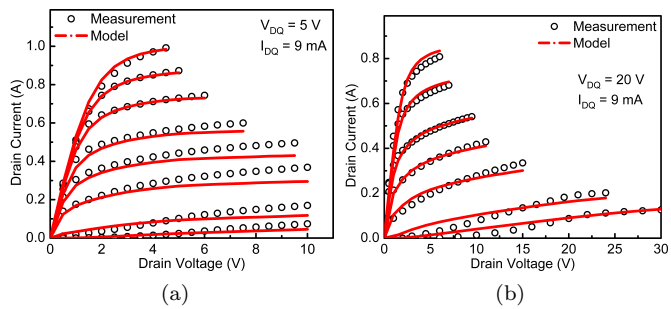

Figure 6: Validation of trap model against pulsed-IV data for two different quiescent conditions; (a) $V_{dq} = 5V$ and (b) $V_{dq} = 20V$.

IV measurements. These effects influence parameters like the sub-threshold slope,cut-off voltage , drain and source-resistances and have been modeled using two RC sub-circuits [15] and have been successfully validated against measured data.

3 Comparison with Measured Data

The ASM-HEMT model has been validated with measured data for source and gate field-plated Toshiba power HEMT and Qorvo RF GaN device. A comparison with measured DC I-V data showing accurate modeling of transfer and output characteristics at multiple drain and gate voltages respectively, as well as at two different temperature conditions (100 °C and -20 °C) is presented in Fig. 3. The model is able to accurately capture the

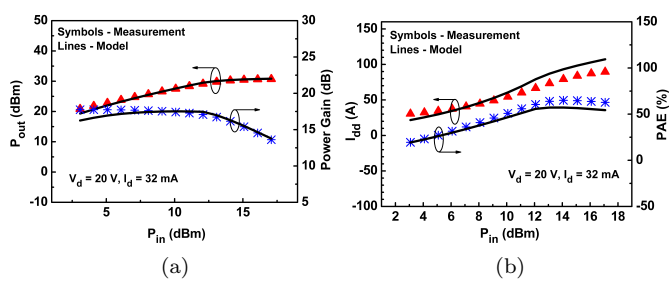

Figure 7: Accurate modeling of (a) RF output power, RF power gain and (b) PAE and bias current Idd (mA), as the input power P_{in} is varied. The drain bias and the input signal frequency is 20 V and 10 GHz, respectively.

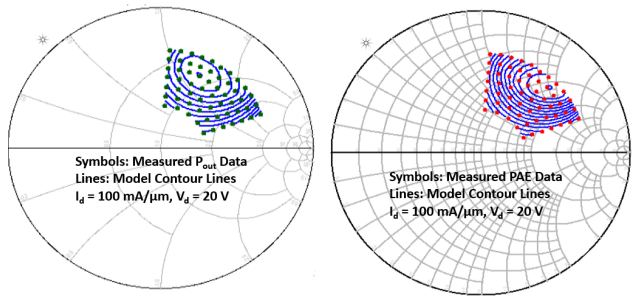

Figure 8: Load pull contour plots for Pout (left) and PAE (right) for bias condition $V_d = 20V$, $Id = 100mA/\mu m$.

effect of non-linear source/drain access region resistance and self-heating at higher gate voltages. Fig. 4 shows the modeling of the output characteristics for RF devices [17] with different widths and number of fingers by scaling the thermal resistance as a key parameter. Effects of gate and source connected FPs on the capacitance behavior for the aforementioned power device are well predicted by the model and presented in Fig. 5(a), (b). The first hump in the $Ciss - V_g$ plot as seen in Fig. 5(a) can be attributed to the intrinsic transistor whereas, the presence of the second hump is due to the gate FP. Gate and source field-plate charges and their cross coupling due to fringing fields engender the off-state capacitances (Ciss, Crss and Coss), the variation of which with V_d is shown in Fig. 5(b). Data from pulsed-IV measurement has been used to extract the parameters related to the trapping effects, which have been modeled as an RC subsection in ASM-HEMT, and the model validation is shown in Fig. 6 for two different quiescent conditions. After completing the DC and trap parameter extraction process, the next step was to extract the parasitic capacitances, inductances and the gate resistance to accurately fit the small-signal S-parameters as well as the large-signal characteristics. The variation in output power (P_{out}), Power Gain, Power-added efficiency (PAE), and Bias current (I_{dd}) for a high drain bias (20V) is presented in Fig. 7. Finally, we validate the model for load-pull contours for two different parameters P_{out} and PAE, shown in Fig. 8.

4 Conclusion

A robust and computationally efficient compact model for GaN HEMT has been presented in the paper. We have validated the performance of the model against measured data from commercial RF and power devices operating under a wide range of bias and temperature conditions. The applicability of the model is corroborated by the fact that it has been selected as an industry standard and will be playing a key role in designing GaN-based circuits for state-of-the-art RF and power applications.

Acknowledgment

This work was partially funded by DST Fast Track Scheme for Young Scientists, ISRO, and CSIR. We would like to thank Toshiba Corporation and Qorvo for providing measurement data as a part of Si2-CMC model standardization activity.

REFERENCES

[1] J. L. Hudgins et al., "An assessment of wide bandgap semiconductors for power devices," in *IEEE TPE*, vol. 18, no. 3, pp. 907-914, May 2003.

[2] I. Angelov et al., "A new empirical nonlinear model for HEMT and MESFET devices," in *IEEE TMTT*, vol. 40, no. 12, pp. 2258-2266, Dec 1992.

[3] O. Jardel et al.,"An Electrothermal Model for AlGaN/GaN Power HEMTs Including Trapping Effects to Improve Large-Signal Simulation Results on High VSWR," in *IEEE TMTT*, vol. 55, no. 12, pp. 2660-2669, Dec. 2007.

[4] U. Radhakrishna et al.,"MIT virtual source GaNFET-RF compact model for GaN HEMTs: From device physics to RF frontend circuit design and validation," 2014 *IEEE IEDM*, CA, USA, 2014, pp. 11.6.1-11.6.4.

[5] S. Khandelwal et al.,"A Physics-Based Analytical Model for 2DEG Charge Density in AlGaN/GaN HEMT Devices," in *IEEE TED*, vol. 58, no. 10, pp. 3622-3625, Oct. 2011.

[6] S. Khandelwal et al., "Analytical Modeling of Surface-Potential and Intrinsic Charges in AlGaN/GaN HEMT Devices," in *IEEE TED*, vol. 59, no. 10, pp. 2856-2860, Oct. 2012.

[7] S-Y Oh et al.,"Transient Analysis of MOS Transistors," in *IEEE JSSC*, vol. 15, no. 4, pp. 636-643, Aug 1980.

[8] S. Khandelwal et al., "A physics based compact model of I-V and C-V characteristics in AlGaN/GaN HEMT devices, *SSE*, vol 76, pp. 60-66, Oct. 2012.

[9] S. Ghosh et al.,"Modeling of source/drain access resistances and their temperature dependence in GaN HEMTs," 2016 *IEEE EDSSC*, Hong Kong, 2016, pp. 247-250.

[10] A. Dasgupta et al., "Compact Modeling of Flicker Noise in HEMTs," in *IEEE JEDS*, vol. 2, no. 6, pp. 174-178, Nov. 2014.

[11] A. Dasgupta et al., "Surface Potential Based Modeling of Thermal Noise for HEMT Circuit Simulation," in *IEEE MWCL*, vol. 25, no. 6, pp. 376-378, June 2015.

[12] A. Dasgupta et al., "Modeling of Induced Gate Thermal Noise in HEMTs," in *IEEE MWCL*, vol. 26, no. 6, pp. 428-430, June 2016.

[13] S. A. Ahsan et al., "Capacitance Modeling in Dual Field-Plate Power GaN HEMT for Accurate Switching Behavior," in *IEEE TED*, vol. 63, no. 2, pp. 565-572, Feb. 2016.

[14] S. A. Ahsan et al.,"Analysis and Modeling of Cross-Coupling and Substrate Capacitances in GaN HEMTs for Power-Electronic Applications," in *IEEE TED*, vol. 64, no. 3, pp. 816-823, March 2017.

[15] S. Ghosh et al., "Analysis and Modeling of Trapping Effects in RF GaN HEMTs under Pulsed Conditions," in *IWPSD*, India, Dec. 2015.

[16] S. A. Ahsan et al., "Physics-Based Multi-Bias RF Large-Signal GaN HEMT Modeling and Parameter Extraction Flow," in *IEEE JEDS*, vol. 5, no. 5, pp. 310-319, Sept. 2017.

[17] Y. Xu et al.,"A Scalable Large-Signal Multiharmonic Model of AlGaN/GaN HEMTs and Its Application in C-Band High Power Amplifier MMIC," in *IEEE TMTT*, vol. 65, no. 8, pp. 2836-2846, Aug. 2017.